BIOCHEMISTRY
including biophysical chemistry & molecular biology

Article

pubs.acs.org/biochemistry

Efficient Delivery of Long-Chain Fatty Aldehydes from the *Nostoc punctiforme* Acyl–Acyl Carrier Protein Reductase to Its Cognate Aldehyde-Deformylating Oxygenase

Douglas M. Warui,[‡] Maria-Eirini Pandelia,[‡] Lauren J. Rajakovich,[†] Carsten Krebs,*[,†,‡] J. Martin Bollinger, Jr.,*[,†,‡] and Squire J. Booker*[,†,‡]

[†]Department of Biochemistry and Molecular Biology, and [‡]Department of Chemistry, The Pennsylvania State University, University Park, Pennsylvania 16802, United States

Supporting Information

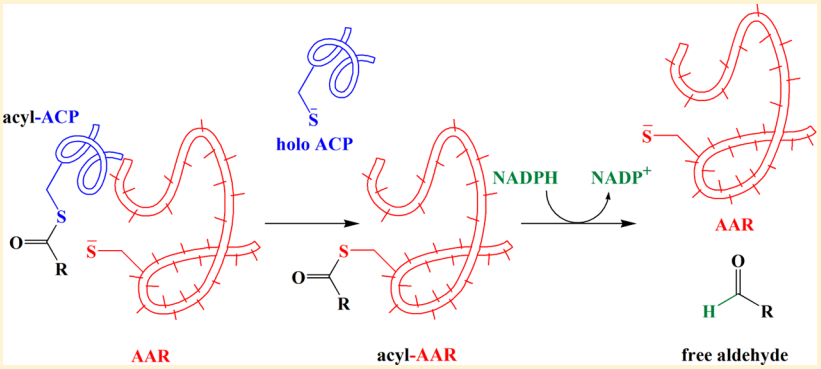

ABSTRACT: A two-step pathway consisting of an acyl–acyl carrier protein (ACP) reductase (AAR) and an aldehyde-deformylating oxygenase (ADO) allows various cyanobacteria to convert long-chain fatty acids into hydrocarbons. AAR catalyzes the two-electron, NADPH-dependent reduction of a fatty acid attached to ACP via a thioester linkage to the corresponding fatty aldehyde, while ADO transforms the fatty aldehyde to a C_{n-1} hydrocarbon and C_1-derived formate. Considering that heptadec(a/e)ne is the most prevalent hydrocarbon produced by cyanobacterial ADOs, the insolubility of its precursor, octadec(a/e)nal, poses a conundrum with respect to its acquisition by ADO. Herein, we report that AAR from the cyanobacterium *Nostoc punctiforme* is activated almost 20-fold by potassium and other monovalent cations of similar ionic radius, and that AAR and ADO form a tight isolable complex with a K_d of 3 ± 0.3 μM. In addition, we show that when the aldehyde substrate is supplied to ADO by AAR, efficient *in vitro* turnover is observed in the absence of solubilizing agents. Similarly to studies by Lin et al. with AAR from *Synechococcus elongatus* [Lin et al. (2013) *FEBS J. 280*, 4773–4781], we show that catalysis by AAR proceeds via formation of a covalent intermediate involving a cysteine residue that we have identified as Cys294. Moreover, AAR specifically transfers the *pro-R* hydride of NADPH to the Cys294-thioester intermediate to afford its aldehyde product. Our results suggest that the interaction between AAR and ADO facilitates either direct transfer of the aldehyde product of AAR to ADO or formation of the aldehyde product in a microenvironment allowing for its efficient uptake by ADO.

The diminishing availability of fossil fuels and the desire to reduce emissions of greenhouse gases and pollutants have led to an increasing interest in the development of safe and renewable alternative energy sources such as solar, wind, hydroelectric, geothermal, hydrogen, and biomass.[1] Although bioethanol and biodiesel are assuming important roles as transportation fuels, the ability to produce hydrocarbons of desired length and branching could provide fuels that better mimic the fossil fuels used currently in the majority of combustion engines.[1−7] In 2010, a two-step pathway for the metabolic production of hydrocarbons from fatty acids in cyanobacteria was reported; it consists of an acyl–acyl carrier protein (ACP) reductase (AAR) and an aldehyde decarbonylase (AD),[8] which we have renamed aldehyde-deformylating oxygenase (ADO) to reflect the true coproduct of the reaction and the important role of dioxygen in catalysis.[9,10] AAR catalyzes an NADPH-dependent two-electron reduction of a C_n fatty acyl–ACP substrate to the corresponding C_n fatty aldehyde, while ADO catalyzes the cleavage of the C_n fatty aldehyde to a C_{n-1} hydrocarbon and the C_1-derived coproduct, formate (Scheme 1). Although the C_1-derived product was not determined in the original report of this two-step pathway, it was assumed to be carbon monoxide (CO),[8,11] shown to be the C_1-derived product in several eukaryotic aldehyde decarbonylases, of which none have been studied in detail *in vitro*.[12−14]

Received: July 9, 2014
Revised: October 25, 2014
Published: December 15, 2014

DOI: 10.1021/bi500847u
Biochemistry 2015, 54, 1006–1015

Scheme 1. Reactions Catalyzed by *Np* AAR and *Np* ADO

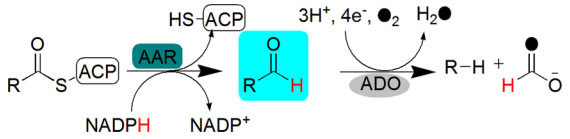

We have shown that *Nostoc punctiforme* (*Np*) ADO, heterologously overproduced in *Escherichia coli* (*Ec*) and purified to homogeneity, produces formate as the C_1-derived coproduct, which is at the same oxidation state as CO (Scheme 1).[15] In later studies, the Marsh laboratory showed that the ADO from *Prochlorococcus marinus* (*Pm*) also yields formate as a coproduct, in what they originally reported was an oxygen-independent reaction.[16,17] Our isotope-tracer studies demonstrated that the aldehydic hydrogen is retained in the formate product and that the hydrogen in the nascent methyl group of the hydrocarbon originates primarily from solvent,[15] which was later also shown for the *Pm* enzyme.[16] Moreover, studies conducted in the presence of $^{18}O_2$ indicated that at least one O_2-derived oxygen atom is incorporated into the formate product, unambiguously establishing the role of dioxygen in the reaction.[9,10] Our more recent studies, which demonstrate that the reaction proceeds via an $Fe_2^{III/III}$-peroxide intermediate, aligns it with other proteins that use a ferritin-like diiron-carboxylate scaffold to bind and activate dioxygen, such as soluble methane monooxygenase (sMMO), the β subunit of class I ribonucleotide reductases, stearoyl-ACP/CoA desaturase, and toluene monooxygenase.[18] Although the activities of *Np* ADO and *Pm* ADO reactions were modest, it was found that turnover is limited by substrate availability, especially when long-chain fatty aldehydes are used as substrates.[15,16]

To date, the majority of *in vitro* mechanistic studies on this two-enzyme system have centered on ADO, with its fatty aldehyde substrate being supplied exogenously. Although ADOs will accept short-chain fatty aldehydes containing as few as seven carbon atoms,[9,17,18] the natural substrates are long-chain fatty aldehydes, with heptadec(a/e)ne and pentadec(a/e)ne being the most prevalent hydrocarbons formed *in vivo*.[8] Both *Np* AAR and *Np* ADO are water-soluble cytoplasmic enzymes: however, the substrates for *Np* ADO are C_{16}- or C_{18}-fatty aldehydes that are poorly soluble in aqueous environments. In *in vitro* activity determinations, the substrate has been artificially solubilized via the inclusion of abiological detergents (e.g., Triton X-100) or dimethyl sulfoxide (DMSO).[9,10,15−17,19] The observed dependence of *in vitro* activity on the inclusion of these abiological agents raises the question: how is the nonpolar fatty aldehyde substrate made available to ADO *in vivo*? Herein, we report the purification of *Np* AAR and show that it is activated ∼20-fold by potassium ions or other monovalent cations with comparable ionic radii. Moreover, *Np* AAR is shown to be able to efficiently supply the fatty aldehyde substrate for *Np* ADO in the absence of agents that solubilize free fatty aldehydes. We have found that *Np* AAR and *Np* ADO form a tight, isolable complex that exhibits a K_d of 3 ± 0.3 μM. Our results corroborate the mechanism proposed in previous studies by Lin et al.[20] that *Np* AAR employs a ping-pong mechanism for catalysis, transferring the acyl group from the acyl−ACP/CoA substrate to an active site cysteinyl residue, which we have identified to be Cys294 in *Np*. Lastly, we show that *Np* AAR selectively catalyzes the transfer of the *pro-R* hydride of NADPH to reduce the thioester linkage of the acyl intermediate and yield the aldehyde product.

EXPERIMENTAL PROCEDURES

Materials. Reduced nicotinamide adenine dinucleotide phosphate (NADPH), bovine liver catalase, $NADP^+$-dependent alcohol dehydrogenase from *Thermoanaerobium brockii*, yeast glucose-6-phosphate dehydrogenase, *Saccharomyces cerevisiae* hexokinase, spinach ferredoxin (F), spinach ferredoxin reductase (FR), tris(2-carboxyethyl) phosphine hydrochloride (TCEP·HCl), phenylmethanesulfonyl fluoride (PMSF), chicken egg white lysozyme, bovine pancreas deoxyribonuclease, and *n*-hexadecane were all obtained from Sigma-Aldrich (St. Louis, MO). Isopropanol-d_8, 1-[^{2}H]-glucose, Coomassie assay protein reagent, and *N*-(2-hydroxyethyl)piperazine-*N*′-2-ethanesulfonic acid (HEPES) were purchased from Fisher Scientific (Pittsburgh, PA), and imidazole was purchased from J. T. Baker Chemical Co (Phillipsburg, NJ). Isopropyl β-D-1-thiogalactopyranoside (IPTG) and dithiothreitol (DTT) were obtained from Gold BioTechnology (St. Louis, MO). TALON metal affinity resin was obtained from Clontech Laboratories Inc. (Mountain View, CA), and Sephadex G-25 resin was obtained from GE-Biosciences (Piscataway, NJ), while DE-52 anion-exchange resin was from Whatman (Florham, NJ). All other buffers and chemicals were of the highest grade available.

General Methods. UV−visible absorption spectra were recorded on a Cary 50 spectrometer from Varian (Walnut Creek, CA) or an Agilent (Foster City, CA) 8453 diode-array spectrometer, both using their associated software for operating the instrument and manipulating the data. Sonic disruption of *Ec* cell suspensions was conducted with a 550 sonic dismembrator from Fisher Scientific using a horn containing a 1/2 in. tip. Overproduction and purification of *Np* ADO, as well as synthesis of *n*-octadecanal were all conducted as previously reported.[15] All buffers were appropriately pH-adjusted using KOH.

Synthesis of Acyl-ACP Substrates. Holo-ACP was prepared by initial phosphopantetheinylation of apo-ACP using *Ec* holo-ACP synthase as previously reported.[21] It was then acylated with a target fatty acid using *Ec* acyl-ACP synthetase. The acylation reaction was performed in acylation buffer (50 mM Tris-HCl, pH 8.0, 20 mM $MgCl_2$, 10 mM ATP, 400 mM LiCl, 2% Triton X-100, and 100 μM TCEP). Upon addition of 200 μM of the fatty acid substrate and 50 μM holo-ACP, the reaction was initiated by the addition of acyl-ACP synthetase to a final concentration of 2 μM and allowed to proceed at 25 °C overnight. The reaction was then diluted 5-fold with 25 mM MES buffer, pH 6.1, and loaded onto a DE-52 column pre-equilibrated in the same buffer. The column was then thoroughly washed with 25 mM MES buffer, pH 6.1, and the acyl-ACP was eluted with a linear gradient from 0 to 850 mM NaCl in 25 mM MES buffer, pH 6.1. Appropriate fractions were identified by the Coomassie protein assay and sodium dodecyl sulfate polyacrylamide gel electrophoresis (SDS-PAGE) and then pooled and concentrated by ultrafiltration. The purified protein was exchanged into gel-filtration buffer (25 mM MES, pH 6.1, 100 mM KCl) using a Sephadex G-25 column. Its purity was determined by SDS-PAGE and/or HPLC, and it was quantified by the Coomassie protein assay using a correction factor of 2.8 determined experimentally.

Synthesis of (4*R*)-[^{2}H]-NADPH. 4*R*-[^{2}H]-NADPH was synthesized as previously described (with minor modifications) by enzymatic reduction of $NADP^+$ with isopropanol-d_8 using a thermostable $NADP^+$ alcohol dehydrogenase from *Thermoanaerobium brockii* (*Tb* ADH).[22] The reaction mixture

DOI: 10.1021/bi500847u
Biochemistry 2015, 54, 1006−1015

contained the following in a total volume of 15 mL: 25 mM Tris−HCl, pH 9.0, 1 M isopropanol-d_8, and 3 mM $NADP^+$. Upon initiation of the reaction by addition of 2 mg (6.5 U) of lyophilized *Tb* ADH, the reaction was gently stirred at 43 °C and monitored for completion by its increase in absorbance at 340 nm. After completion (~30 min), the reaction mixture was chilled on ice and then filtered through a 10 kDa membrane after addition of 100 mg KCl. The filtrate was flash-frozen in liquid nitrogen and lyophilized. The lyophilized yellowish powder was dissolved in minimal HPLC buffer A (20 mM ammonium acetate, 0.1 M KCl, pH 8.0) and purified on a semipreparative Zorbax C18 (9.4 × 250 mm) column with detection by absorbance at 340 nm using a 60 min isocratic gradient of 95% buffer A and 5% buffer B (100% methanol) at a flow rate of 0.4 mL/min. The purified (4*R*)-[^{2}H]-NADPH was reanalyzed for purity on a Zorbax SB C18 analytical column (4.6 × 250 mm, 5 μm) with detection by absorbance at 340 nm using a 30 min isocratic gradient of 95% buffer A and 5% buffer B at a flow rate of 0.25 mL/min. The (4*R*)-[^{2}H]-NADPH product, which was found to be ≥95% pure, was flash-frozen in liquid nitrogen and lyophilized. The lyophilized material was stored at −20 °C until it was used.

Synthesis of (4*S*)-[^{2}H]-NADPH. 4*S*-[^{2}H]-NADPH was synthesized as previously described (with minor modifications) by enzymatic reduction of $NADP^+$ with 1-[^{2}H]-glucose 6-phosphate using yeast glucose-6-phosphate dehydrogenase. The 1-[^{2}H]-glucose 6-phosphate was generated *in situ* from 1-[^{2}H]-glucose by yeast hexokinase.[23] The reaction mixture contained the following in a total volume of 30 mL: 50 mM Tris-HCl, pH 7.5, 7 mM $MgCl_2$, 3.5 mM ATP, 2.5 mM $NADP^+$, and 5 mM 1-[^{2}H]-glucose. Upon initiation of the reaction by addition of 2 mg of lyophilized hexokinase and 0.8 mg of lyophilized glucose-6-phosphate dehydrogenase, the reaction was incubated at 25 °C, with monitoring of NADPH formation by absorbance at 340 nm. Upon completion (30−45 min), the reaction mixture was diluted 10-fold with ice-chilled water and applied (in the dark at 4 °C) to a Sephadex DEAE A25 column (30 × 65 mm) that had been charged with 1 M KCl in 5 mM Tris-HCl and further equilibrated in 5 mM Tris-HCl, pH 7.5. After the reaction mixture was loaded, the column was first washed with 0.5 L of 5 mM Tris-HCl, pH 7.5, before NADPH was eluted with a 0.5 L linear gradient of 0−0.7 M KCl in 5 mM Tris-HCl, pH 7.5. Fractions (5 mL) containing NADPH were identified by their absorbance at 340 nm, and were pooled and flash-frozen in liquid nitrogen and lyophilized. The purity of the (4*S*)-[^{2}H]-NADPH was determined to be ≥95% by analytical HPLC, as described above. The lyophilized (4*S*)-[^{2}H]-NADPH was stored at −20 °C until it was used.

Preparation of *Np* AAR Enzyme. The gene encoding *Np* AAR, codon-optimized for expression in *Ec*, was supplied by GeneArt (Regensburg, Germany) and subsequently subcloned into the *Nde*I and *Eco*RI restriction sites of expression vector pET-26b. Upon verification of the correct sequence at the Penn State University Molecular Core Sequencing Facility, the plasmid, designated pNpAARwt-md, was used to transform into *Ec* BL21(DE3) along with plasmids pG-KJE8 or pG-Tf2 (Clontech Laboratories Inc., Mountain View, CA), which encode molecular chaperones. Gene expression and protein overproduction were conducted at 37 °C in shake flasks containing Luria−Bertani (LB) medium supplemented with 25 μg/mL kanamycin, 12.5 μg/mL chloramphenicol and 5 ng/mL tetracycline (pG-TF2), or 5 ng/mL tetracycline and 2 mg/mL L-arabinose (pG-KJE8). *Np* AAR expression was induced at an OD_{600} of 0.8 by addition of IPTG to a final concentration of 100 μM, and was allowed to proceed at 30 °C for 3 h with shaking (180 rpm) before the cells were harvested by centrifugation at 6,000 × *g*. The resulting cell paste was frozen in liquid nitrogen and stored at −80 °C until it was used. All purification steps were performed at 4 °C unless noted otherwise. In a typical purification, 30 g of cell paste was resuspended at room temperature in 150 mL of lysis buffer (50 mM potassium phosphate, pH 8.0, 300 mM KCl, 10% glycerol, 2% Triton X-100 and 1 mM TCEP). Lysozyme and deoxyribonuclease were both added to final concentrations of 0.1 mg/mL, and the suspension was incubated on ice for an additional 30 min. PMSF, dissolved in a minimal volume of ethanol, was then added to a final concentration of 0.5 mM, and the cells were subjected to four 1-min bursts of sonic disruption at a setting of 7 while on ice with 8 min of cooling following each sonic burst. The cell lysate was then centrifuged at ≥20,000 × *g* at 4 °C for 30 min. The supernatant was loaded onto a TALON metal affinity resin column pre-equilibrated in lysis buffer. The resin was washed with wash buffer (50 mM potassium phosphate, pH 8.0, 300 mM KCl, 10% glycerol, 1 mM TCEP, and 20 mM imidazole) before the protein was eluted with 50 mM potassium phosphate, pH 8.0, 300 mM KCl, 10% glycerol, 4 mM TCEP, and 250 mM imidazole. The purified protein was exchanged into gel-filtration buffer (50 mM HEPES, pH 7.6, 250 mM KCl, 10% glycerol, and 5 mM TCEP) by using a Sephadex G-25 column. Protein concentration was determined by absorbance at 280 nm using a calculated extinction coefficient of 37,930 M^{-1} cm^{-1} (http://ca.expasy.org).

Site-Directed Mutagenesis of *Np* AAR. The C35S, C63S, C139S, C161S, C240S, and C249S single variants of *Np* AAR were constructed by using the Stratagene QuikChange II kit (Agilent Technologies) with plasmid pNpAARwt-md as the template and primers listed in Table S1. Target base changes were analyzed by sequencing, and the variant proteins were overproduced and purified as described above for the wild-type protein.

Enzymatic Assays. Most assays (see amendments in the figure legends) were conducted at 37 °C in a final volume of 100 μL and contained the following components at their indicated final concentrations where appropriate: 1 μM *Np* AAR, 2.5 μM *Np* ADO, 200 μM *Ec* stearoyl-ACP, 500 μM octadecanal, 2 mM NADPH, 100 mM KCl, 20 μg spinach ferredoxin, 5 mU spinach ferredoxin reductase, 100 U catalase, 0.2% Triton X-100, 5 mM TCEP, and 50 mM HEPES, pH 7.6. For analysis of the alkane and aldehyde reaction products, assays were quenched and extracted by addition of an equal volume of HPLC grade ethyl acetate containing 50 μM hexadecane as an internal standard. Extracted samples were analyzed on a Shimadzu GCMS-QP5000 gas chromatograph mass spectrometer as previously reported.[15] For formate quantification, samples were derivatized and analyzed on an Agilent QQQ 6410 LC/MS instrument as previously reported.[15]

Size-Exclusion Chromatography. Size-exclusion chromatography was conducted on an ÄKTA purification system (GE Healthcare Biosciences, Pittsburgh, PA) fitted with a HiPrep 16/60 Sephacryl S-200 HR gel-filtration column equilibrated in a buffer containing 10 mM HEPES, pH 7.5, 150 mM NaCl, 5 mM DTT, and 10% glycerol at a flow rate of 0.5 mL/min. Aliquots (250 μL) of *Np* AAR (200 μM) and *Np* ADO (200 μM) or a mixture of the two (200 μM each) were applied to

DOI: 10.1021/bi500847u
Biochemistry 2015, 54, 1006−1015

the column, and the elution volumes of the individual proteins or the complex of the proteins were determined and compared to a standard curve generated from the elution volumes of ribonuclease A, ovalbumin, conalbumin, β-amylase, and blue dextran.

Determination of Dissociation Constants by Isothermal Titration Calorimetry. Binding of *Np* AAR to *Np* ADO and *Ec* stearoyl-ACP was quantified at 25 °C by isothermal titration calorimetry (ITC) using a MicroCal Auto-ITC200 microcalorimeter (GE Healthcare Biosciences, Pittsburgh, PA). Protein samples were thoroughly exchanged into binding buffer (10 mM potassium phosphate buffer, pH 7.6, 100 mM KCl, and 2 mM TCEP) by gel-filtration chromatography and ultrafiltration. *Np* AAR was placed into the Auto-iTC200 sample cell (200 μL working volume) at a final concentration of 28 μM and was titrated against *Np* ADO (418 μM) or *Ec* stearoyl-ACP (280 μM) using 1 μL injections of each ligand. Each binding analysis was accompanied by a control experiment in which the ligand was titrated into the sample cell containing only the titration buffer. Before the data were fitted, the control raw data were subtracted from the corresponding raw titration data to account for the heat associated with ligand dilution. The corrected data were processed with the Origin 7 software package (GE Healthcare Biosciences, Pittsburgh, PA).

RESULTS

Cloning, Expression, and Purification of *Np* AAR. To generate the cognate reductase for *Np* ADO, the genomic DNA sequence that encodes *Np* AAR (*Np*un_R1710) was codon-optimized for gene expression in *E. coli*, synthesized, and cloned into the *Nde*I and *Eco*RI restriction sites of expression vector pET-28a by GeneArt (Regensburg, Germany). This construct, in which gene expression is under the control of a T7 promoter, allows overproduction of the protein with an N-terminal hexahistidine (His_6) tag separated from its native start codon by a spacer of 10 amino acids. The resulting plasmid, designated pNpAARwt, was used to transform *Ec* BL21 (DE3) for gene expression and protein overproduction; however, the protein overproduced in this fashion was largely insoluble. In an attempt to generate soluble protein, the *Np aar* gene was subcloned into the *Nde*I and *Eco*RI restriction sites of expression vector pET-26b, which generates a C-terminal His_6-tag separated from the last native amino acid by a 14-amino acid spacer. The gene on this plasmid, designated, pNpAARwt-md, was coexpressed with genes on one of two plasmids (pG-KJE8 or pG-Tf2) that encode for molecular chaperones. The pG-KJE8 plasmid encodes DnaK, DnaJ, GrpE, GroES, and GroEL, while plasmid pG-Tf2 encodes GroES, GroEL, and trigger factor. It was observed that the chaperones led to a 3- to 5-fold enhancement in yield of *Np* AAR. The protein was purified by immobilized metal affinity chromatography to ≥95% homogeneity as determined by SDS-PAGE (Figure S1A, Supporting Information). Its UV−vis absorption spectrum, shown in Figure S1B, exhibits no significant absorbance at 260 nm and at wavelengths beyond 300 nm, suggesting that the purified protein is devoid of any known organic cofactors. Yields of *Np* AAR varied from 1−2 mg of protein per gram of cell paste.

Measurements of *Np* AAR Activity. *Np* AAR was not the subject of the original study by Schirmer et al., who studied *Np* ADO and the AAR from *Synechococcus elongatus* (*Se*). In that study, *Se* AAR was found to catalyze reduction of fatty acids linked either to ACP or coenzyme A (CoA). Although the V_{max} for the reaction using the CoA-linked fatty acid substrate (19.8 μmol/L·h) was more than twice that observed when using the ACP-linked fatty acid (7.6 μmol/L·h), the K_M value for the former was 15-fold greater than that of the latter. The greater k_{cat}/K_M value suggests that the *in vivo* substrate is an ACP-linked fatty acid. It should be noted, however, that, in their kinetic analyses, the *Se* AAR never catalyzed even one full turnover. Nevertheless, from the concentration of enzyme used in their activity determinations (10 μM), a $V_{max}/[E_T]$ value of 0.01−0.03 min^{-1} can be estimated.[8] When the activity of *Np* AAR was measured under conditions similar to those described by Schirmer et al., very little (∼ one turnover) production of the corresponding fatty aldehyde was observed after 24 h of incubation at room temperature, although a similar Michaelis−Menten plot could be constructed, which afforded a K_M value of 27 ± 6 μM for stearoyl−ACP and a turnover number of 0.02 min^{-1}. As described below, this turnover number improved markedly when potassium was included in the assays, increasing to 0.17 min^{-1}, while the K_M value remained essentially constant (24 ± 5 μM) (Figure S2A).

Effect of Catalase on *Np* ADO and *Np* AAR Activities. Recently, Marsh and co-workers showed that *Se* AAR, which they referred to as *Se* acyl CoA reductase (*Se* ACR), is activated ∼10-fold by potassium ions.[20] Our own studies allowed us to arrive at a similar conclusion via a somewhat circuitous, but important, pathway. Studies from the Shanklin laboratory showed that *Pm* ADO is strongly inhibited by hydrogen peroxide, which is generated because of the inefficient delivery of reducing equivalents from the exogenous reducing system (F/FR/NADPH) during turnover, and that catalase (CAT) can prevent or reverse this inhibition.[19] In fact, the authors showed that an ADO/CAT construct, in which CAT was genetically fused to the C-terminus of ADO, afforded significantly greater turnovers than ADO alone *in vitro*, and also *in vivo* when the gene that encodes it was coexpressed with the gene encoding *Se* AAR.[19] Based on these findings, we assessed whether CAT might have a similar effect on *Np* ADO, and found that it does (blue and red lines in Figure S2B), either when the fatty aldehyde substrate is added exogenously as octadecanal or when it is supplied via the *Np* AAR reaction (black line in Figure S2B).

Surprisingly, when 20 μM *Np* AAR was incubated with 200 μM stearoyl-ACP under turnover conditions (4 mM NADPH, 10 mM HEPES, pH 7.6, 2 mM $MgSO_4$, and 10 mM DTT) in the presence of 100 U CAT, but in the absence of *Np* ADO, formation of the aldehyde product was enhanced 14-fold compared to the reactions that lacked CAT (Figure 1A). Given that *Np* AAR is not expected to generate peroxide during turnover, this result suggested that some component in the CAT preparation enhances *Np* AAR activity. To show convincingly that CAT, itself, was not responsible for the enhanced *Np* AAR activity, it was exchanged into HEPES buffer, pH 7.6, by gel-filtration chromatography before being used in activity assays. As shown in Figure 1B (black bars), CAT that was exchanged into HEPES buffer was ineffective at enhancing the activity of both *Np* AAR and *Np* ADO when *Np* AAR and *Ec* stearoyl-ACP were used as the source of the aldehyde substrate. By contrast, when the CAT solution was filtered through a centrifugal concentrator with a 3 kDa molecular weight cutoff membrane, the filtrate was effective in enhancing the *Np* AAR reaction but not the *Np* ADO reaction (Figure 1B, red bars). In this latter instance, the lack of an effect on the *Np* ADO reaction, even when the aldehyde substrate

DOI: 10.1021/bi500847u
Biochemistry 2015, 54, 1006−1015

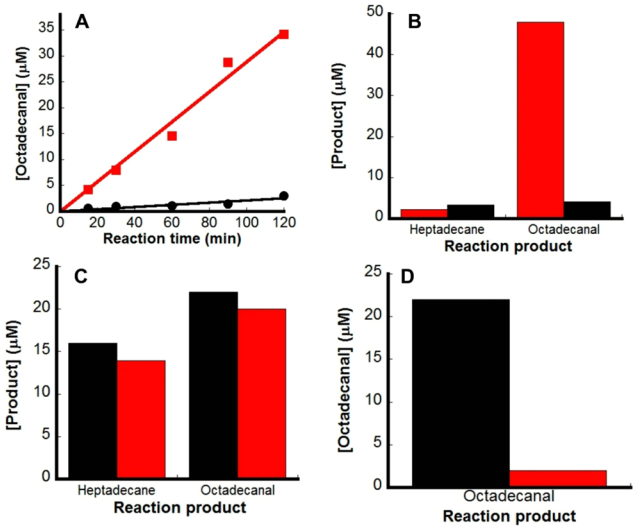

Figure 1. Effect of bovine catalase on the *Np* AAR and *Np* ADO reactions. (A) Activity of *Np* AAR (20 μM) in the absence (black) or presence (red) of 100 U of CAT. (B) Activity of *Np* AAR and *Np* ADO in the presence of CAT that was exchanged into HEPES buffer, pH 7.6 (black bars), or in the presence of the filtrate obtained from concentrating CAT in a centrifugal device with a 3 kDa cutoff (red bars). (C) Activity of *Np* AAR and *Np* ADO in the presence of CAT filtrate that was boiled for 10 min (red bars) or in the presence of unheated CAT filtrate (black bars). (D) Activity of *Np* AAR in the presence of a CAT filtrate that was treated with Chelex-100 (red bar) or in the presence of untreated CAT filtrate (black bar). Reactions in (B)–(D) were carried out at 37 °C for 90 min prior to analysis.

was being generated via an active *Np* AAR reaction, derives from the absence of CAT, which relieves inhibition of the *Np* ADO by peroxide.

The above results provide strong evidence that the factor enhancing *Np* AAR activity is a small molecule or ion. To identify this factor, the CAT filtrate was first boiled for 10 min to destroy any heat-sensitive organic molecules. When the boiled filtrate was used in activity assays (Figure 1C, red bars), it was essentially as effective in enhancing the *Np* AAR activity as the unheated CAT filtrate (Figure 1C, black bars). When the CAT filtrate was treated with Chelex-100 instead, a resin that binds metal ions, its ability to enhance the *Np* AAR reaction was abrogated (Figure 1D, red bar) as compared to that of the untreated CAT filtrate (Figure 1D, black bar), suggesting that a metal ion is responsible for the enhanced activity.

Identification of the Metal Ion that Activates *Np* AAR Activity. To identify the metal ion responsible for *Np* AAR activation, metal analysis by inductively coupled plasma atomic emission spectroscopy (ICP-AES) was carried out on the CAT solution. As observed in Table S2, Al^{3+}, K^+, Na^+, Fe^{3+} and Mn^{2+} were present at the highest concentrations. Na^+ was eliminated from further consideration on the basis that it had already been included (as a buffer component) at substantial concentrations in *Np* AAR assay mixtures.

When Li^+, Na^+, Ag^+, K^+, Fe^{2+}, Fe^{3+}, Mn^{2+}, Al^{3+}, Ca^{2+}, Co^{2+}, or Zn^{2+} was included in *Np* AAR activity determinations, K^+ dramatically enhanced the activity of the protein, while the remaining metals had little (Li^+ and Na^+) or no effect (Figure 2A). To assess whether monovalent cations with ionic radii similar to that of K^+ (1.52 Å) might also enhance *Np* AAR activity, activity assays were carried out in the presence of 100 mM K^+, Rb^+ (1.66 Å), Cs^+ (1.81 Å), or NH_4^+ (1.61 Å) ions. The activities in the presence of K^+, Rb^+, and NH_4^+ were similar, while the activity in the presence of Cs^+, a monovalent cation with a significantly greater ionic radius, was noticeably diminished (Figure 2B). By contrast, metal ions with significantly lesser ionic radii, such as Li^+ (0.90 Å), Na^+ (1.16 Å), or Ag^+ (1.29 Å) had little to no effect on the reaction (Figure 2A). Further analysis of concentration dependencies of the effect of K^+, NH_4^+, and Rb^+ on the *Np* AAR reaction showed that the metal ions supported maximal activity when they were present at concentrations of ~200 mM. At higher concentrations, the metal ions were inhibitory (Figure 2C–E). The use of chloride as the counterion in all of the salts employed indicates that the stimulatory effect observed with some of the salts is correlated to the cation rather than the anion.

***Np* AAR Can Efficiently Supply *Np* ADO with Its Substrate.** To determine whether *Np* AAR can efficiently supply the aldehyde substrate for *Np* ADO, the activity of *Np* ADO was measured under four different conditions: in the presence of 500 μM octadecanal (Figure 3A, violet line), 500 μM octadecanal and 0.2% Triton X-100 (Figure 3A, blue line), 500 μM octadecanal and 5% DMSO (Figure 3A, black line), and in the presence of stearoyl-ACP and the *Np* AAR aldehyde-generating system (Figure 3B). In the presence of 500 μM octadecanal and CAT, 2.5 μM *Np* ADO catalyzed relatively rapid production of ~2.5 μM heptadecane within 10 min of incubation at 37 °C; however, the concentration of heptadecane did not increase significantly after that period of time. When the same reaction was conducted in the presence of 0.2% Triton X-100, production of ~17 μM heptadecane was observed after a 3 h incubation period. Turnover in the presence of DMSO afforded a similar result (~14 μM heptadecane formed). By contrast, in a reaction containing 1 μM *Np* AAR and 2.5 μM *Np* ADO, formation of almost 40 μM heptadecane and 20 μM free octadecanal, respectively, was

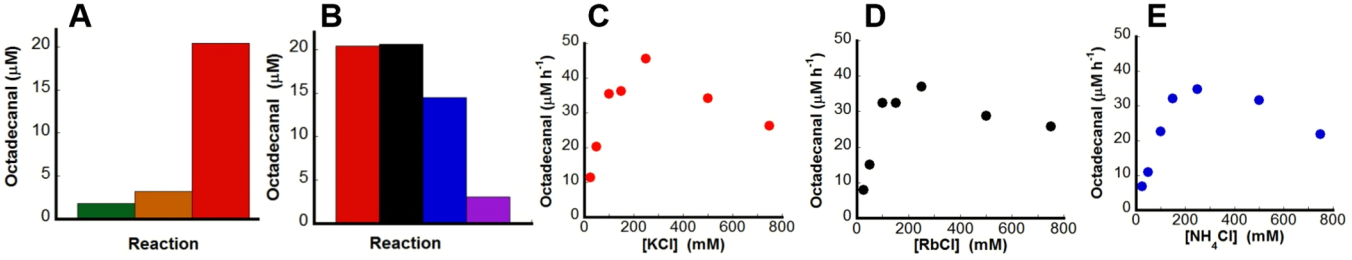

Figure 2. (A) Effect of various metal ions (Li^+, Na^+, Ag^+, K^+, Fe^{2+}, Fe^{3+}, Mn^{2+}, Al^{3+}, Ca^{2+}, Co^{2+}, or Zn^{2+}) added to 100 mM final concentration on *Np* AAR activity. Only the addition of Li^+ (green), Na^+ (orange), or K^+ (red) led to any measurable activity. (B) Presence of 100 mM K^+ (red), Rb^+ (black), NH_4^+ (blue), or Cs^+ (purple). Determination of K_M for (C) KCl, (D) RbCl, and (E) NH_4Cl.

DOI: 10.1021/bi500847u
Biochemistry 2015, 54, 1006–1015

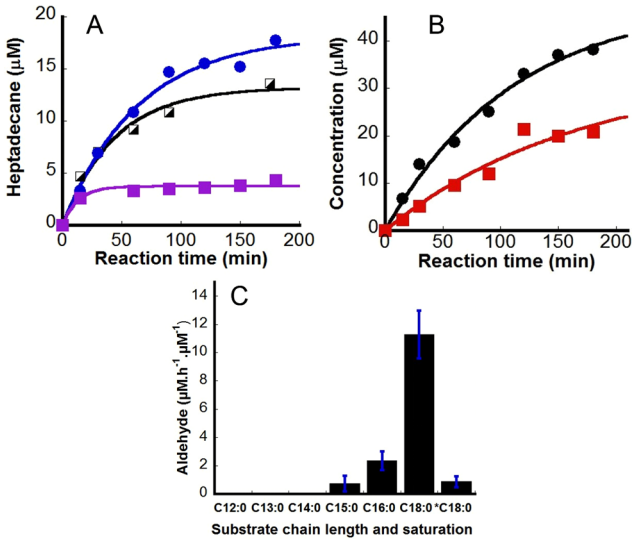

Figure 3. Delivery of the aldehyde substrate to *Np* ADO in the absence (A) and presence (B) of *Np* AAR. (A) No solubilizing agent (violet squares); 0.2% Triton X-100 (blue circles); 5% DMSO (black squares). (B) Octadecanal product (red squares) and heptadecane product (black circles). Conditions: CAT (100 U), KCl (100 mM), *Np* ADO (2.5 μM), *Np* AAR (1 μM), octadecanal (500 μM), and *Ec* stearoyl-ACP (200 μM). (C) Substrate chain-length specificity for *Np* AAR using C12 to C18 acyl-ACPs (C12:0−C18:0) and C18-acyl-CoA (*C18:0). Conditions: KCl (200 mM), AAR (2 μM), acyl-ACP (100 μM), and acyl-CoA (100 μM).

observed after incubation for 3 h at 37 °C. The sum of the heptadecane and free octadecanal (60 μM) represents the total concentration of octadecanal produced by the *Np* AAR over the designated incubation period.

It was also observed that, under turnover conditions, the presence of *Np* ADO stimulates the activity of *Np* AAR; given that the rate of product formation and the total concentration of product for *Np* AAR were enhanced when *Np* ADO was present (0.51 min^{-1}, ∼ 40 μM after 30 min) (Figure S2D) compared to when it was absent (0.39 min^{-1}, ∼22 μM after 30 min) (Figure S2C). Although the presence of *Np* AAR led to enhanced alkane production, the initial rate for *Np* ADO-dependent heptadecane production was not significantly affected compared to when the substrate was provided exogenously, suggesting that *Np* ADO is rate-limiting in this two-enzyme system. It should also be noted that substrate/product inhibition was evident in *Np* AAR steady-state reactions when acyl-ACP concentration was greater than 200 μM, though this inhibition was somewhat relieved in the presence of *Np* ADO undergoing turnover (Figure S3).

Investigation of the *Np* AAR Substrate Specificity. Because *Np* AAR catalyzes the first committed step in this pathway for hydrocarbon formation, it is important to delineate the factors governing its substrate specificity. As shown in Figure 3C, *Np* AAR has a preference for long-chain substrates, with a C18 fatty acyl group supporting the highest activity. This finding corroborates previous *in vivo* studies when AAR and ADO from *Se* were heterologously coexpressed in *Ec*.[8] In addition, fatty acyl groups containing 14 carbon atoms or fewer, were not detectably converted to the C_{n-1} hydrocarbon. Given that *Np* ADO as well as the *Pm* ADO are known to act on fatty aldehydes containing at least seven carbon atoms,[9,17,18] this result suggests that AAR sets the substrate chain-length specificity for ADO. Lastly, our results indicate that *Np* AAR has a strong preference for acyl−ACP substrates over acyl-CoA substrates as was reported previously for *Se* AAR, given that the C18 acyl-CoA substrate was turned over inefficiently in comparison with the C18 acyl-ACP.[8]

***Np* AAR and *Np* ADO Form a Stable Complex.** Given the effect of *Np* AAR activity on the *Np* ADO turnover, various experiments were designed to assess whether the two proteins form a stable or transient complex. Figure 4A shows an analysis

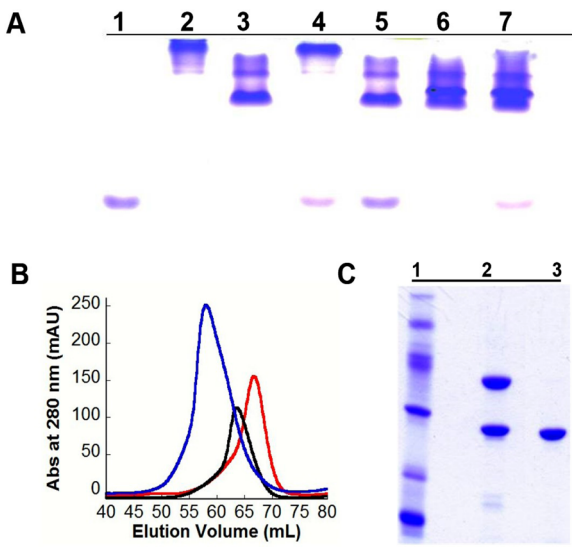

Figure 4. (A) Clear-native PAGE analysis showing complex formation between *Np* AAR and *Np* ADO. Lane 1, *Ec* oleoyl-ACP (184 μM); lane 2, *Np* AAR (100 μM); lane 3, *Np* ADO (100 μM); lane 4, *Np* AAR (100 μM) + oleoyl ACP (184 μM); lane 5, *Np* ADO (100 μM) + oleoyl-ACP (184 μM); lane 6, *Np* AAR (100 μM) + *Np* ADO (100 μM); lane 7, *Np* AAR (100 μM) + *Np* ADO (100 μM) + oleoyl-ACP (184 μM). (B) Elution profile of 200 μM each, *Np* AAR (red), *Np* ADO (black) and *Np* AAR + Np ADO (blue) by size-exclusion chromatography. (C) SDS-PAGE of *Np* AAR plus *Np* ADO complex when *Np* AAR was mixed with excess *Np* ADO; lane 1 is protein molecular weight markers; lane 2 is FPLC fraction corresponding to 1:1 *Np* AAR:ADO complex and lane 3 is the fraction corresponding to the excess *Np* ADO.

of the interaction between *Np* ADO and *Np* AAR, as well as *Np* AAR and *Ec* oleoyl-ACP. *Ec* oleoyl-ACP migrates most rapidly (pI = 3.98) and *Np* AAR migrates least rapidly (pI = 6.27). *Np* ADO migrates at an intermediate distance toward the upper half of the gel (pI = 5.49), and also displays a second, weaker band of higher molecular mass (lanes 1−3). At present, we attribute the lower band (lane 3) to a monomeric *Np* ADO species, whereas the upper band represents a dimeric species. When *Ec* oleoyl−ACP and *Np* AAR are combined, the staining of the fast-migrating oleoyl-ACP band is diminished, consistent with its binding to *Np* AAR, which is present at a lower concentration (lane 4). When oleoyl-ACP is combined with *Np* ADO, no significant change in staining or migration of either protein is observed, suggesting that the two proteins do not directly interact (lane 5). By contrast, when *Np* AAR and *Np* ADO are combined, the slow-migrating *Np* AAR band is completely titrated away, and a new band migrating just above the stronger of the two *Np* ADO-derived bands is observed, demonstrating the formation of a complex between the two pathway enzymes (lane 6).

Figure 4B depicts a calibrated size-exclusion chromatographic elution profile showing the interaction between *Np* AAR (MW

DOI: 10.1021/bi500847u
Biochemistry 2015, 54, 1006−1015

= 39,813) and *Np* ADO (MW = 28,467) . When *Np* AAR is chromatographed alone, it migrates as a protein of molecular mass 33,672 Da, which is most consistent with a monomeric state in solution. When *Np* ADO is chromatographed alone, it migrates as a protein of molecular mass of 40,408 Da, which we suggest is a dimeric species, in line with other ferritin-like diiron-carboxylate proteins. Dynamic light scattering experiments were further conducted. They confirmed that *Np* AAR exists as a monomer with an experimental molecular mass of 46,000 Da and that *Np* ADO exists as a homodimer with an experimental molecular mass of 54,000 Da. When the two proteins are preincubated in equivalent amounts before being subjected to size-exclusion chromatography, a new faster-eluting peak is observed, which displays migratory properties of a complex of molecular mass 58,189 Da, consistent with a 1:1 complex of *Np* AAR:ADO. Figure 4C depicts SDS−PAGE analysis of two distinct fractions from size-exclusion chromatography of the *Np* ADO + *Np* AAR mixture (*Np* ADO in excess). As observed, the faster-migrating peak contains both AAR and ADO (lane 2), consistent with a complex of the two, while the slower-migrating peak (lane 3) corresponds to the excess *Np* ADO. This result is consistent with a 1:1 complex formed between *Np* AAR and *Np* ADO.

To characterize the complex between *Np* AAR and *Np* ADO further, the thermodynamics of association was quantified by ITC. Figure 5A shows representative data for the titration of

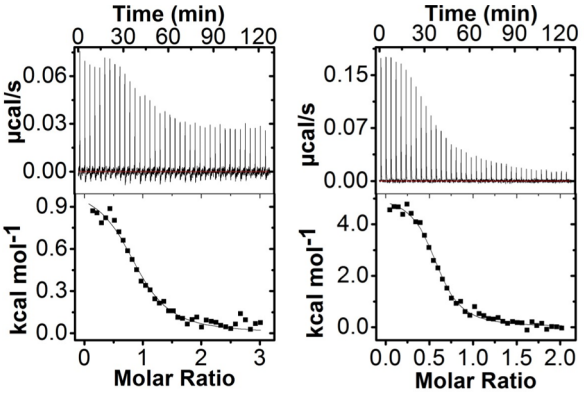

Figure 5. Representative ITC binding data for *Np* ADO titrated into *Np* AAR (A) and *Ec* stearoyl-ACP titrated into *Np* AAR (B). Top panels represent the raw titration data, in which each peak depicts the heat absorbed upon addition of the titrant. Bottom panels reflect the corrected experimental injection heats (squares) derived from the integration of the corresponding heat bursts (top panels), while the continuous lines reflect the calculated fits of the data to a single-site binding model in each case.

Np ADO into a solution of *Np* AAR, from which a K_d of 3 ± 0.3 μM was deduced, while Figure 5B shows representative data for titration of stearoyl-ACP into a solution of *Np* AAR, from which a K_d of 1.2 ± 0.1 μM was deduced. The ITC data reveal that *Np* AAR·ADO and *Np* AAR·ACP interactions are both endothermic, and thus entropically driven.

***Np* AAR Reaction Mechanism Involves Formation of a Stable Acyl-Enzyme Intermediate.** Previous studies by Lin et al. indicated that *Se* AAR catalyzes its reaction via an acyl-enzyme intermediate,[20] most likely involving a conserved cysteine residue on the enzyme. Given that this study was conducted with an acyl-CoA substrate rather than an acyl-ACP substrate, we assessed whether *Np* AAR operates via a similar ping-pong mechanism when acting on acyl-ACP substrates. *Np* AAR was incubated with 1-[^{13}C]-stearoyl-ACP in the absence of NADPH, and the mixture was then analyzed by electrospray ionization (ESI)-mass spectrometry (ESI-MS). In Figure 6B (bottom), the zero-charge transformed mass spectrum of *Np* AAR in the absence of substrate exhibits a molecular mass of 39,817 Da, in good agreement with the theoretical molecular mass of 39,812.79 Da. By contrast, when *Np* AAR was incubated with the acyl-ACP substrate prior to analysis, a $\Delta(m/z)$ of +269 was observed, which is consistent with addition of a ^{13}C-labeled octadecanoyl moiety (theoretical MW 268 + 1) (Figure 6B (top). This observation suggests that the *Np* AAR reaction involves formation of an acyl-enzyme intermediate before reduction of the fatty acyl group, as was deduced by Lin et al. for the *Se* AAR homologue.[20]

Identification of *Np* AAR Active-Site Cysteine by Site-Directed Mutagenesis and ESI-MS Analysis. Given that transient enzyme thioester linkages are often found in enzymatic reactions that involve the transfer of a fatty acyl group from acyl-ACP or acyl-CoA to a second substrate via a ping-pong reaction, as well as the finding by Lin et al. that the *Se* AAR is inhibited by iodoacetamide,[20] we hypothesized that a cysteine residue participates in the acyl-enzyme intermediate in the *Np* AAR reaction. *Np* AAR has a total of six cysteines, of which all were individually targeted for replacement with serine to assess the effect of the substitution on enzyme turnover and the ability to form a covalent intermediate. Figure 6A depicts activity determinations on these Cys → Ser variant enzymes. All variants, except the C294S, exhibited modest to strong activity, suggesting that only C294 plays an intimate role in catalysis. To confirm that C294 is the active-site residue that undergoes transient acylation, the variant protein was incubated in the presence and in the absence of 1-[^{13}C]-stearoyl-ACP and analyzed by ESI-MS. In contrast to that of the wild-type protein, the mass spectrum of the C294S variant shows no evidence for acylation (Figure 6C). When incubated with or without the acyl-ACP substrate its zero-charge transformed mass spectrum displayed a MW of 39,798 in close agreement with the theoretical MW of 39,796.

***Np* AAR is A-Side Specific with Respect to NADPH.** In a reaction containing both *Np* AAR and *Np* ADO under turnover conditions, the C_n-aldehyde produced by the *Np* AAR reaction is subsequently taken up by *Np* ADO as substrate to yield a C_{n-1}-hydrocarbon and C1-derived formate that retains the aldehydic hydrogen.[9,10,15] To determine whether the hydride incorporated into the aldehyde product by *Np* AAR comes directly from NADPH and from which face of NADPH it originates, reactions were carried out with NADPH stereoselectively labeled with one deuterium at C4. If *Np* AAR is A-side specific and the reaction is performed in the presence of (4*R*)-[^{2}H]-NADPH, then a deuteride would be incorporated into the aldehyde product, whereas an unlabeled hydride would be incorporated instead if the *pro-S* hydride were to be transferred. Alternatively, if *Np* AAR is B-side specific, a deuteride should be incorporated in the aldehyde product when (4*S*)-[^{2}H]-NADPH is used, while an unlabeled hydride would be incorporated if the *pro-R* hydride were transferred. Therefore, both (4*S*)-[^{2}H]-NADPH and (4*R*)-[^{2}H]-NADPH were synthesized enzymatically and incubated with *Np* AAR and *Np* ADO under turnover conditions and the formate product was analyzed by LC-MS. As shown in Figure 7 (black bar), deuterium incorporation was observed in the formate product only when (4*R*)-[^{2}H]-NADPH was used. When (4*S*)-

DOI: 10.1021/bi500847u
Biochemistry 2015, 54, 1006−1015

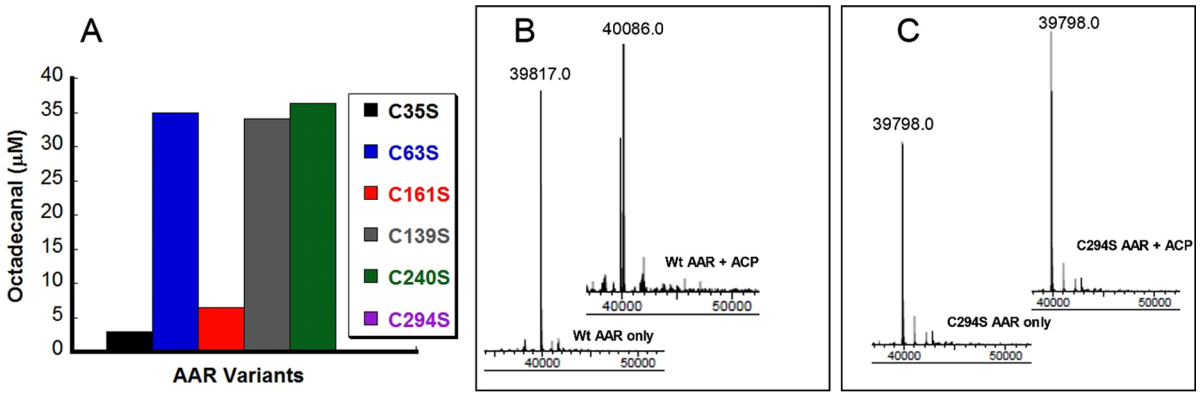

Figure 6. (A) Activity measurements for *Np* AAR Cys → Ser variants. All reactions were performed in parallel under identical conditions, and consisted of 4 μM of the *Np* AAR variant, 200 μM stearoyl-ACP, and 2 mM NADPH. Reactions were incubated at 37 °C for 30 min prior to analysis for aldehyde product by GC-MS. (B) Zero-charge-transformed ESI-MS spectra of wt *Np* AAR in the absence (bottom chromatogram) and in the presence of 1-[^{13}C]-stearoyl-ACP (top chromatogram). (C) Zero-charge-transformed ESI-MS spectra of *Np* AAR C294S in the absence (bottom chromatogram) and presence of stearoyl-ACP (top chromatogram).

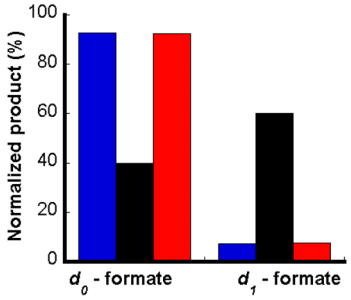

Figure 7. LC-MS analysis of unlabeled and deuterium-labeled formate coproduct of *Np* ADO from reactions in which *Np* AAR was used to supply the aldehyde substrate via stearoyl-ACP. The results are for unlabeled NADPH (blue bar), (4*R*)-[^{2}H]-NADPH (black bar), and (4*S*)-[^{2}H]-NADPH (red bar).

[^{2}H]-NADPH was used under similar conditions, deuterium was not incorporated in the formate product (Figure 7, red bar). *Np* ADO turnover requires the input of electrons, which, in our assays, are supplied by the F/FR/NADPH reducing system. In this reducing system, FR catalyzes the reversible reduction of F with concomitant oxidation of NADPH to NADP$^+$. Reduction of NADP$^+$ to NADPH is expected to lead to transfer of a hydride from solvent and thus result into deuteride-hydride scrambling in (4*R*)-[^{2}H]-NADPH (Scheme 2), which is in accordance with the results of our assays that

Scheme 2. Reversibility of the Reaction Catalyzed by FR That Ultimately Would Lead to Deuterium-Hydride Scrambling in NADPH

$$2\,F_{ox} + NADPH \underset{}{\overset{FR}{\rightleftharpoons}} 2\,F_{red} + NADP^+ + H^+$$

showed less than the expected transfer of the deuteride from (4*R*)-[^{2}H]-NADPH. Nevertheless, our results clearly demonstrate that *Np* AAR is stereospecific and transfers only the *pro-R* hydride of NADPH.

DISCUSSION

Unlike partially characterized ADs from eukaryotes, which are mostly membrane associated,[12,13] cyanobacterial ADOs are soluble in aqueous solution. By contrast, the preferred substrate for cADOs, a C18 fatty aldehyde, is sparingly soluble in the same milieu, begging the question: how is the fatty aldehyde substrate made available to the ADO *in vivo*? One mechanism for substrate acquisition that we imagined is that a physical association, either stable or transient, between AAR and ADO might allow a direct transfer of the product of the AAR reaction into the active site of ADO. Our studies herein focused on *Np* AAR, both because all of our previous mechanistic work was conducted on the ADO from the same organism and because previous studies had shown that *Np* ADO afforded the highest level of hydrocarbons in *Ec* when the gene encoding it was coexpressed with one encoding AAR.[8]

As detailed by Lin et al., who were unable to purify and characterize this enzyme, *Np* AAR is highly insoluble when overproduced in *Ec*. However, we were able to purify milligram quantities of the enzyme when it was overproduced in the presence of several chaperones. Although the original characterization of *Se* AAR by Schirmer et al. indicated that this enzyme operated both on ACP- and CoA-derived fatty acyl groups,[8] the study by Lin et al. did not address ACP-linked substrates[20] and gave the impression that its true substrate is a CoA-derived fatty acyl group, in contrast to the conclusion reached by Schirmer et al.[8] Our studies herein on *Np* AAR clearly establish that its substrate is ACP-linked and that CoA-linked fatty acyl groups are poor substrates. As already established by Lin et al. for the *Se* AAR, *Np* AAR is maximally active in the presence of potassium ions, and other monovalent cations of comparable atomic radii can also activate to varying extents. Although we discovered this potassium requirement serendipitously, a subsequent search of the literature indicated that many aldehyde dehydrogenases, which catalyze oxidation of aldehydes to their corresponding acids, have potassium-binding sites of unknown function.[24] At present, we do not understand the role of the metal ion in *Np* AAR: it could be structural in nature, as observed for the aldehyde dehydrogenases,[24] or it might play a more intimate role in catalysis.

It is difficult to assess from the work of Lin et al. how many turnovers the *Se* AAR catalyzes *in vitro*; however, under our best conditions, *Np* AAR catalyzed more than 25 turnovers within 1 h in the presence of *Np* ADO undergoing turnover (heptadecane + octadecanal). Moreover, when the fatty aldehyde was supplied by *Np* AAR, *Np* ADO catalysis can proceed without exogenous addition of reagents that solubilize long-chain fatty aldehydes. In fact, the extent of *Np* ADO

DOI: 10.1021/bi500847u
Biochemistry 2015, 54, 1006−1015

turnover in the presence of *Np* AAR was almost twice that for *Np* ADO operating alone in the presence of Triton X-100 or DMSO to solubilize the exogenously added octadecanal substrate. Formation of both octadecanal and heptadecane begins to level off after only 10−20 turnovers, which may be due to severe product inhibition. Studies to pinpoint the factors behind this inactivation might provide crucial insights into engineering this system to generate useful quantities of hydrocarbons.

Given the higher level of *Np* ADO turnover in the presence of *Np* AAR, we assessed whether the two enzymes might form a complex, which could allow direct transfer of the fatty aldehyde intermediate from *Np* AAR to the active site of *Np* ADO. An interaction between *Np* ADO and *Np* AAR was shown by clear-native PAGE as well as size-exclusion chromatography, and the interaction was strong enough that the complex could be isolated and shown by SDS-PAGE to contain the two proteins in a 1:1 ratio. Further studies by ITC indicated that the complex containing the two proteins exhibits a K_d of ∼3 μM, and that complex formation is entropically driven.

At present we do not know whether *Np* AAR channels its fatty aldehyde product directly into the *Np* ADO active site or whether it simply helps maintain a constant supply of soluble aldehyde in solution. When the fatty aldehyde is provided exogenously, the majority of it is expected to be present in micelles, which explains the very small, but relatively rapid (as compared to assays containing additives), amount of turnover that we observe in the absence of detergent when using long-chain fatty aldehydes as substrates. In fact, the amount of turnover that we observe in the absence of additives or the *Np* AAR aldehyde generating system suggests that the critical micelle concentration for octadecanal is ∼3−5 μM. When *Np* ADO converts the free fatty aldehydes to alkanes, the re-establishment of an equilibrium concentration of free aldehyde is quite slow on the time scale of enzyme turnover. During overnight incubations, however, significantly more of the fatty aldehyde substrate is turned over as fatty aldehydes are slowly released from micelles, which results in a reaction time course that resembles burst kinetics. Given that the substrate for the *Np* ADO reaction is provided by *Np* AAR, our results set the stage for a variety of detailed *in vitro* studies of this two-enzyme system that might lead to an enhancement of its efficiency as well as the production of customized alkanes from renewable sources.

■ ASSOCIATED CONTENT

Supporting Information

Ec codon-optimized DNA sequence encoding *Np* AAR, Figures S1−S3, and Tables S1 and S2. This material is available free of charge via the Internet at http://pubs.acs.org

■ AUTHOR INFORMATION

Corresponding Authors

*(S.J.B.) Mailing address: 302 Chemistry Building, The Pennsylvania State University, University Park, PA 16802. Phone: 814-865-3014. Fax: 814-865-2927. Email: Squire@psu.edu.

*(C.K.) Mailing address: 332 Chemistry Building, The Pennsylvania State University, University Park, PA 16802. Phone: 814-865-6089. Fax: 814-865-2927. E-mail: ckrebs@psu.edu.

*(J.M.B.) Mailing address: 336 Chemistry Building, The Pennsylvania State University, University Park, PA 16802. Phone: 814-883-1464. Fax: 814-865-2927. E-mail: jmb21@psu.edu.

Funding

This work was supported by the National Science Foundation (MCB-1122079 to C.K., J.M.B, and S.J.B.).

Notes

The authors declare no competing financial interest.

■ ACKNOWLEDGMENTS

Technical assistance from Mr. Henry Gong (ICP-AES), Dr. Neela Yennawar and Julia Fecko (DLS and ITC), and James Miller (mass spectrometry) is gratefully acknowledged.

■ ABBREVIATIONS

ACP, acyl carrier protein; AAR, acyl−acyl carrier protein reductase; AD, aldehyde decarbonylase; ADO, aldehyde-deformylating oxygenase; CAT, catalase; DMSO, dimethyl sulfoxide; DTT, dithiothreitol; *Ec*, *Escherichia coli*; ESI, electrospray ionization; F, spinach ferredoxin; FR, spinach ferredoxin reductase; HEPES, 2-[4-(2-hydroxyethyl)piperazin-1-yl]ethanesulfonic acid; ICP-AES, inductively coupled plasma atomic emission spectroscopy; IPTG, isopropyl β-D-1-thiogalactopyranoside; ITC, isothermal titration calorimetry; MES, 2-(*N*-morpholino)ethanesulfonic acid); $NADP^+$, oxidized nicotinamide adenine dinucleotide phosphate; NADPH, reduced nicotinamide adenine dinucleotide phosphate; *Np*, *Nostoc punctiforme*; PMSF, phenylmethylsulfonyl fluoride; SDS-PAGE, sodium dodecyl sulfate polyacrylamide gel electrophoresis; *Se*, *Synechococcus elongatus*; *Tb*, *Thermoanaerobium brockii*; Tris, tris(hydroxymethyl)aminomethane

■ REFERENCES

(1) Committee on America's Energy Future (2009) *America's Energy Future: Technology and Transformation*, National Academies Press, Washington, D.C..

(2) Radakovits, R., Jinkerson, R. E., Darzins, A., and Posewitz, M. C. (2010) Genetic Engineering of Algae for Enhanced Biofuel Production. *Eukaryotic Cell 9*, 486−501.

(3) Wackett, L. P. (2010) Engineering microbes to produce biofuels. *Curr. Opin. Biotechnol. 22*, 1−6.

(4) Ducat, D. C., Way, J. C., and Silver, P. A. (2011) Engineering cyanobacteria to generate high-value products. *Trends Biotechnol. 29*, 95−103.

(5) Zhang, F. Z., Rodriguez, S., and Keasling, J. D. (2011) Metabolic engineering of microbial pathways for advanced biofuels production. *Curr. Opin. Biotechnol. 22*, 775−783.

(6) Rabinovitch-Deere, C. A., Oliver, J. W. K., Rodriguez, G. M., and Atsumi, S. (2013) Synthetic biology and metabolic engineering approaches to produce biofuels. *Chem. Rev. 133*, 4611−4632.

(7) Serrano-Ruiz, J. C., Ramos-Fernández, E. V., and Sepúlveda-Escribano, A. (2012) From biodiesel and bioethanol to liquid hydrocarbon fuels: new hydrotreating and advanced microbial technologies. *Energy Environ. Sci. 5*, 5638−5652.

(8) Schirmer, A., Rude, M. A., Li, X. Z., Popova, E., and del Cardayre, S. B. (2010) Microbial Biosynthesis of Alkanes. *Science 329*, 559−562.

(9) Li, N., Chang, W.-c., Warui, D. M., Booker, S. J., Krebs, C., and Bollinger, J. M., Jr. (2012) Evidence for only oxygenative cleavage of aldehydes to alk(a/e)nes and formate by cyanobacterial aldehyde decarbonylases. *Biochemistry 51*, 7908−7916.

(10) Li, N., Nørgaard, H., Warui, D. M., Booker, S. J., Krebs, C., and Bollinger, J. M., Jr. (2011) Conversion of fatty aldehydes to alka(e)nes and formate by a cyanobacterial aldehyde decarbonylase: cryptic redox by an unusual dimetal oxygenase. *J. Am. Chem. Soc. 133*, 6158−6161.

DOI: 10.1021/bi500847u
Biochemistry 2015, 54, 1006−1015

(11) Schirmer, A., Rude, M. A., and Brubaker, S. (2009) Methods and compositions for producing hydrocarbons. Patent WO 2009140696 A3.
(12) Cheesbrough, T. M., and Kolattukudy, P. E. (1984) Alkane biosynthesis by decarbonylation of aldehydes catalyzed by a particulate preparation from *Pisum sativum*. *Proc. Natl. Acad. Sci. U. S. A. 81*, 6613−6617.
(13) Dennis, M., and Kolattukudy, P. E. (1992) A cobalt-porphyrin enzyme converts a fatty aldehyde to a hydrocarbon and CO. *Proc. Natl. Acad. Sci. U. S. A. 89*, 5306−5310.
(14) Krebs, C., Bollinger, J. M., Jr., and Booker, S. J. (2011) Cyanobacterial alkane biosynthesis further expands the catalytic repertoire of the ferritin-like "di-iron-carboxylate" proteins. *Curr. Opin. Chem. Biol. 15*, 291−303.
(15) Warui, D. M., Li, N., Nørgaard, H., Krebs, C., Bollinger, J. M., Jr., and Booker, S. J. (2011) Detection of formate, rather than carbon monoxide, as the stoichiometric coproduct in conversion of fatty aldehydes to alkanes by a cyanobacterial aldehyde decarbonylase. *J. Am. Chem. Soc. 133*, 3316−3319.
(16) Das, D., Eser, B. E., Han, J., Sciore, A., and Marsh, E. N. G. (2011) Oxygen-independent decarbonylation of aldehydes by cyanobacterial aldehyde decarbonylase: A new reaction of diiron enzymes. *Angew. Chem. Int. Ed. 51*, 7881−7881.
(17) Eser, B. E., Das, D., Han, J., Jones, P. R., and Marsh, E. N. G. (2011) Oxygen-independent alkane formation by non-heme iron-dependent cyanobacterial aldehyde decarbonylase: investigation of kinetics and requirement for an external electron donor. *Biochemistry 50*, 10743−10750.
(18) Pandelia, M.-E., Li, N., Nørgaard, H., Warui, D. M., Chang, W.-c., Rajakovich, L. J., Booker, S. J., Krebs, C., and Bollinger, J. M., Jr. (2013) Substrate-triggered addition of dioxygen to the diferrous cofactor of aldehyde-deformylating oxygenase to form a diferric-peroxide intermediate. *J. Am. Chem. Soc. 135*, 15801−15812.
(19) Andre, C., Kim, S. W., Yu, X.-H., and Shanklin, J. (2013) Fusing catalase to an alkane-producing enzyme maintains enzymatic activity by converting the inhibitory byproduct H_2O_2 to the cosubstrate O_2. *Proc. Natl. Acad. Sci. U. S. A. 110*, 3191−3196.
(20) Lin, F., Das, D., Lin, X. N., and Marsh, E. N. G. (2013) Aldehyde-forming fatty acyl-CoA reductase from cyanobacteria: expression, purification and characterization of the recombinant enzyme. *FEBS J. 280*, 4773−4781.
(21) Nesbitt, N. M., Baleanu-Gogonea, C., Cicchillo, R. M., Goodson, K., Iwig, D. F., Broadwater, J. A., Haas, J. A., Fox, B. G., and Booker, S. J. (2005) Expression, purification, and physical characterization of *Escherichia coli* lipoyl(octanoyl)transferase. *Protein Expression Purif. 39*, 269−282.
(22) Jeong, S. S., and Gready, J. E. (1994) A Method of Preparation and Purification of (4*R*)-Deuterated-Reduced Nicotinamide Adenine Dinucleotide Phosphate. *Anal. Biochem. 221*, 273−277.
(23) Wilken, D. R., King, H. L., and Dyar, R. E. (1975) Ketopantoic acid and ketopantoyl lactone reductases. Stereospecificity of transfer of hydrogen from reduced nicotinamide adenine dinucleotide phosphate. *J. Biol. Chem. 250*, 2311−2314.
(24) Garza-Ramos, G., Mújica-Jiménez, C., and Muñoz-Clares, R. A. (2013) Potassium and Ionic Strength Effects on the Conformational and Thermal Stability of Two Aldehyde Dehydrogenases Reveal Structural and Functional Roles of K^+-Binding Sites. *PLoS One 8*, e54899.

DOI: 10.1021/bi500847u
Biochemistry 2015, 54, 1006−1015